AIAA JOURNAL
Vol. 46, No. 3, March 2008

Periodic Forcing of the Turbulent Boundary Layer on a Body of Revolution

Vladimir I. Kornilov* and Andrei V. Boiko†
Russian Academy of Sciences, 630090, Novosibirsk, Russia

DOI: 10.2514/1.28829

The effect of local periodic forcing in the form of blowing/suction through a transverse annular slot on the properties of a turbulent boundary layer formed on an axisymmetric body of revolution in an incompressible flow is studied experimentally. The Reynolds number based on the momentum thickness of the boundary layer in front of the annular slot is 1348. The dimensionless amplitude of the forced signal A_0 was set to be 0.2, 0.3, and 0.4. The frequency of the forced signal in wall units was varied within $f^+ = 0.0051$–0.0126. The slot width s^+ in wall units was 47. A permanent decrease in local skin friction, reaching up to 70%, is observed to occur at a distance from the slot approximately equal to half a displacement thickness δ^*, followed by the recovery of the skin friction to the undisturbed value at $25\delta^*$.

Nomenclature

A_0	=	forcing amplitude
C_f	=	local skin-friction coefficient
C_P	=	static-pressure coefficient, $(P - P_\infty)/q_\infty$
f	=	forcing frequency
H	=	boundary-layer shape factor, $H = \delta^*/\theta$
L	=	overall length of the body of revolution
P_∞	=	reference static pressure
q	=	dynamic pressure, $\rho U^2/2$
R	=	lateral radius of curvature
Re_θ	=	Reynolds number based on U_∞ and θ
s	=	width of the slot
U_∞	=	reference freestream velocity
u'	=	streamwise velocity fluctuation
v_*	=	friction velocity, $v_* = \sqrt{\tau_w/\rho}$
x	=	streamwise coordinate, distance from the body nose
y	=	wall-normal coordinate, distance from the wall
Δx	=	downstream distance from the slot
δ	=	boundary-layer 99% thickness
δ^*	=	boundary-layer displacement thickness
θ	=	boundary-layer momentum thickness
ν	=	kinematic viscosity
ρ	=	density
τ	=	wall shear stress

Subscripts

bl	=	blowing conditions
e	=	boundary-layer edge conditions
f	=	at a given *frequency*
suc	=	suction conditions
w	=	wall conditions
0	=	slot location conditions or total pressure
∞	=	freestream conditions

Superscripts

$\overline{()}$	=	time-averaged value
$+$	=	normalization by wall units

I. Introduction

PROGRESS in understanding the phenomenon of coherent structures in wall-bounded turbulent flows and mechanisms responsible for the formation of such structures [1] stimulates further research aimed at studying the possibility of reducing the drag of a moving object, especially the skin-friction component. Examples of coherent structures include counter-rotating vortices in two-dimensional turbulent wakes, large-scale vortex structures in turbulent mixing layers, and low-speed streaks and hairpin vortices in turbulent boundary layers. Higher values of turbulent friction are often associated with the downward motion of fluid induced by streamwise vortices (coherent structures) developing near the surface [2]. These vortices, which differ in size and shape interact with the viscous sublayer and thus form flow regions with elevated shear stresses. There are two principally different approaches for controlling the near-wall turbulent flows. The first one can be considered as a measure for preventing the aforementioned vortices. The second approach is aimed at attenuating the intensity of these vortices. There is one more approach, which consists in the jet injection into the incoming boundary layer and insertion of new vortices under the existing layer. Effective control over these vortices can be a key element of a successful strategy for turbulent skin-friction reduction. As an example of such an approach, which currently attracts particular attention, one can use blowing/suction through the wall in the form of zero net mass flux jet. Publications on this topic show that this type of flow control, depending on parameters of forcing and body configuration, can reduce local friction, ensure more efficient separation control, and even improve the lifting properties of such a configuration [3–10].

In early research, the efforts of most authors were focused on studying the effectiveness of steady actuations. Park and Choi [3] showed that steady blowing through a flat wall can reduce friction and increase turbulence intensity, whereas steady suction produces the opposite effect. They found that steady local blowing lifts the streamwise vortices, weakening their interaction with the wall. As a result, friction decreases in the vicinity of the slot, and turbulence intensity and friction increase further downstream from the slot. A significant decrease in friction in the vicinity of the slot can be reached even with comparatively low values of blowing and suction velocities: less than $0.1U_\infty$. It was also shown that the Reynolds stress components acquire their initial values at larger distances from the slot in the downstream direction than the streamwise component of velocity fluctuations. Park et al. [4] found that small local periodic

Received 14 November 2006; revision received 3 November 2007; accepted for publication 3 November 2007. Copyright © 2007 by the American Institute of Aeronautics and Astronautics, Inc. All rights reserved. Copies of this paper may be made for personal or internal use, on condition that the copier pay the $10.00 per-copy fee to the Copyright Clearance Center, Inc., 222 Rosewood Drive, Danvers, MA 01923; include the code 0001-1452/08 $10.00 in correspondence with the CCC.

*Assistant Professor and Leading Scientist, Department of Experimental Aerogasdynamics, Khristianovich Institute of Theoretical and Applied Mechanics, Siberian Branch.

†Assistant Professor and Leading Scientist, Department of Aerophysical Studies of Subsonic Flows, Khristianovich Institute of Theoretical and Applied Mechanics, Siberian Branch.

forcing through a transverse slot on a flat plate decreases friction, whereas the effectiveness of the control increases with the forcing frequency. It is important that turbulence intensity appeared to be only slightly higher than that for a regular boundary layer, except for the flow region immediately downstream of the slot. That paper seems to demonstrate the most suitable example of periodic forcing, because, in contrast to the experiments [5], the authors managed to provide a zero net mass flux through the slot. It is not accidental that the effect reached in [4] is markedly more pronounced. It is shown in [5], nevertheless, that continuous and periodic blowing can be effectively used to reduce local friction. It was later confirmed in [6] that the maximum reduction of turbulent friction can be reached at the highest examined forcing frequency ($f^+ = 0.088$) and with a slot manufactured at an angle of -120 deg to the flow.

Controlling periodic blowing/suction through a transverse slot in the wall of a flat plate in a water channel was also ensured in [7]. Stable reduction of friction drag (about 18%) was noted, which was estimated by the mean velocity gradient near the wall. A stable increase in turbulence intensity in the entire measurement region downstream of the slot was simultaneously observed.

The majority of numerical research was focused on studying the effectiveness of steady actuations. Sano and Hirayama [8] used this control method to investigate the possibility of delaying flow separation and found that steady blowing decreases friction, whereas steady suction increases friction, so that the turbulence intensity behaves in the opposite manner. Kim et al. [9] used direct numerical simulation to study the influence of steady local blowing with three different blowing velocities on the boundary layer. Particular attention was paid to ensure conditions of a constant mass flow rate through the slot. The effectiveness of periodic blowing through a transverse slot on a two-dimensional boundary layer was also considered in [10] by numerical methods. The time-averaged blowing velocity was within 10% of the external flow velocity, and the frequency of forced oscillations was fixed and equal to $f^+ = 0.017$. The results obtained by the authors were compared with similar data for continuous blowing. It was shown that a significant decrease of the friction in the vicinity of the slot (reaching 80%) was obtained. This value was found to be somewhat lower in the case of periodic blowing.

The present paper describes an experimental study of effectiveness of local periodic forcing in the form of blowing/suction of varied frequency and amplitude on a turbulent boundary layer formed on an axisymmetric body of revolution. The study was motivated by the following considerations. The papers previously cited dealt with the effect of continuous and periodic blowing/suction on a turbulent boundary layer formed on a flat surface. In some cases [4,5,10], as was previously noted, such a method of flow control was demonstrated to be extremely effective. Yet, as far as the authors are aware, no such studies were performed for fuselagelike bodies. It is these configurations, however, that are of much practical interest. Unlike, for example, wing surfaces, on which an extended region of laminar flow normally arises and for which a broad range of control methods is available, the boundary layer on bodies of revolution is turbulent almost from the very beginning of its development; this boundary layer is therefore hard to manipulate. Moreover, it is not obvious that the results obtained on a flat surface can be transferred to the flow around a body of revolution.

II. Experimental Conditions and Procedure

The tests were carried out in the closed-return subsonic low-turbulent wind tunnel with the test section that has a cross-sectional area of 1×1 m and 4-m length; in most tests, the freestream velocity in the reference cross section was $U_\infty = 10.1$ m/s. In this case, the Reynolds number Re_θ based on the momentum thickness in the cross section located 13 mm upstream from the annular slot was 1348. Also, some tests on the initial configuration (with no blowing/suction) were carried out at higher flow velocities: up to 25 m/s. These experiments were undertaken to check whether the boundary layers at higher velocities were in the Clauser equilibrium state.

The experiments were performed on a body of revolution of length $L = 2586$ mm (Fig. 1). This model is sting-mounted in the test section of the wind tunnel on a rigid pylon. The model consists of a leading part, which is an ellipsoid, for which the major semi-axis is 300 mm, and a cylindrical part that is 100 mm in diameter.

To ensure a developed turbulent flow on the major part of the model, the boundary layer on the model is artificially tripped. This is done using a boundary-layer tripping ring made of a wire that is 1.5 mm in diameter (44 in wall units $d^+ = d\upsilon_*/\nu$), positioned 270 mm downstream of the nose of the body, and a 80-mm-long strip of Stayer sandpaper with no. 60 grit size. The sandpaper strip was installed downstream of the tripping ring to reduce the two-dimensional characteristics of the ring. To avoid problems with model bending and to suppress vibrations that could emerge in the flow, the model is provided with an additional streamlined support. Twenty static-pressure orifices that are 0.4 mm in diameter are located along a generatrix of the body of revolution. In addition, a J-type thermocouple (produced by Agilent Technologies) was also mounted at a distance of 1050 mm from the nose of the body of revolution.

Local blowing/suction was performed through an oblique annular slot located at a distance of 1030 mm ($\bar{x} = x/L = 0.398$) downstream from the nose of the body of revolution. Such a location of the slot was chosen based on preliminary studies that showed that an equilibrium turbulent boundary on the test model tested might be expected, starting from this distance. Although the width of the slot s in the streamwise direction was adjustable, the experiments were carried out at a constant 1.6-mm width in the streamwise direction. This quantity in wall units $s^+ = s\upsilon_*/\nu$ was 47 and was chosen to be roughly equal to the typical streamwise size of the main energy-containing vortices. It is clear that the turbulent energy in a boundary layer is mainly carried by the large-scale structures that scale with the layer thickness and is of the order of 0.1δ. According to this, the width of the slot in our case is larger than

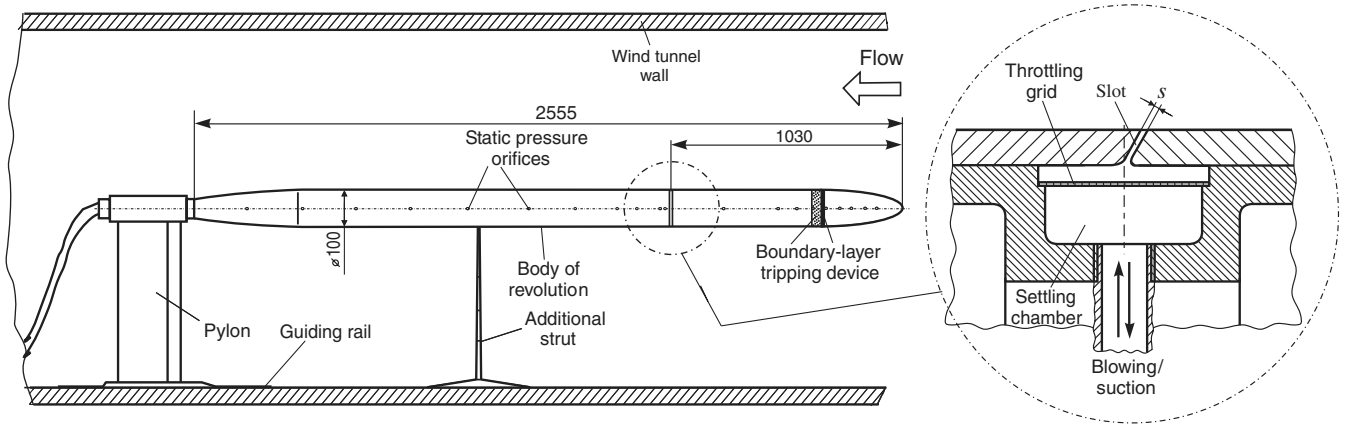

Fig. 1 Body of revolution schematic and annular slot geometry, not to scale; all dimensions are in millimeters.

the value chosen for s^+. On the other hand, a wide slot is a disturbance source for a boundary layer. Taking this consideration into account, the final value s^+ was chosen as a compromise between these two factors. The forcing angle was chosen to be $-120°$, which provides the greatest effect of skin-friction reduction, as was shown in [6], based on data for a flat plate.

Particular attention was paid to providing a uniform distribution of localized blowing/suction in the circumferential direction of the body of revolution. For this purpose, there was a common settling chamber directly under the slot, which was separated from the slot by a grid with a system of throttling orifices that are 0.5 mm in diameter. Pulsed actuation into the settling chamber and then to the slot and back was driven by a dynamic loudspeaker with a power of 25 W located outside the wind-tunnel test section. The loudspeaker was connected by a smooth reinforced hose (with an inside diameter of 28 mm) with an annular channel of smooth geometry, which ensured access to 16 radial holes that are 8 mm in diameter and are aligned at an angle of 22.5 deg to each other and then to the common settling chamber. The dynamic loudspeaker performance was controlled by a U7-1 power amplifier and a G3-33 generator of acoustic oscillations with a sinusoidal output of controlled frequency f and amplitude A of the forced signal. With no flow in the test section, the values of f and A were monitored at the slot output at a distance $y = 0.5$ mm from the wall. A hot-wire probe with a single sensor was preliminary calibrated in the external flow to obtain its velocity and angular characteristics. The range of flow velocities in calibrations was much greater than that reached in the experiments. The data obtained show that the probe used is insensitive (within a 5% mistake) to the flow pitching angles up to 40 deg. A miniature standard microphone was also used to control the sinusoidal signal performance at the slot output.

Detailed measurements of the wall-normal velocity of the forced jet v_f over the slot width at a distance of 0.5 mm from the wall were performed with no external flow. Concerning the accuracy of these measurements, the following should be noted. It is known that single hot wires do not give information about flow direction. In the presence of periodic blowing/suction, it must be guessed as to whether the wall-normal velocity is negative or positive. In addition, in the overlap region near zero velocity, the response curve of the hot wire is highly nonlinear and strongly affected by free convection. The probe employed was not calibrated near zero velocity, because this procedure was extremely difficult. For this reason, the data around the zero crossings could not be measured with great care. In our case, the internal geometry of the slot has smooth contours, in contrast to the shape toward the external flow. Hence, it is reasonable to believe that the amplitude of the forced signal at the phase of blowing is higher than that at the phase of suction. Indeed, the jet flow was found to be asymmetric over the slot width (approximately 15%), which indicates that blowing/suction is obviously performed in a nonoptimal manner. However, at the maximum point, the measured wall-normal velocity due to the local forcing has a shape close to a typical sinusoid $v_f(t) = (v_f)_{\max} \sin(2\pi f t)$ (Fig. 2), where t is the time and $T = 1/f$ is the period of oscillations. The rigorous symmetry between the phases of blowing and suction through the slot could not be ensured in the present experiments. A possible reason is the specific features of the slot geometry, which has smooth contours joining the settling chamber, whereas such a shape is naturally impossible toward the external flow. As a consequence, there are different dynamic losses in the slot entrance outside and inside model walls and, correspondingly, the signal in the phase of blowing is not quite identical to that in the phase of suction. This also can be caused by the basic difference between a sink and a source. During the process of suction the slot behaves almost like a two-dimensional potential flow sink, in which the flow is constant over a semicircle. Hence, the suction velocity at height y above the slot is proportional to $v_{\text{suc}} \approx q/\pi y$, where q is the volume flow rate per unit width. A 2D jet expands at a much lower rate (e.g., $b = ky$, where k is a number less than 1). Hence, the blowing velocity at the same elevation will be $v_{\text{bl}} \approx q/ky$, and so one could expect the peak suction and blowing velocities to differ by a factor $v_{\text{suc}}/v_{\text{bl}} \approx k/\pi < 1$.

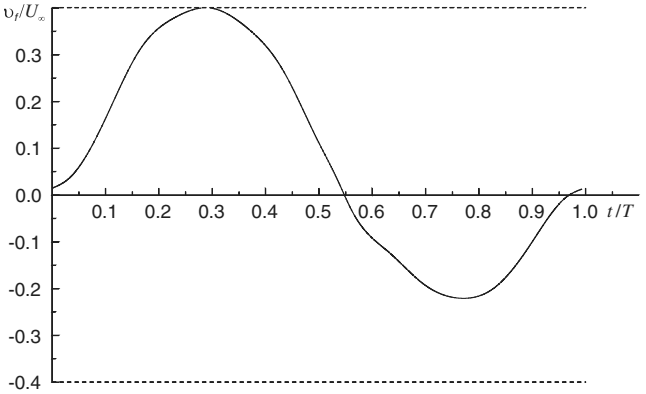

Fig. 2 Measured wall-normal velocity for $f^+ = 0.0051$ and $A_0 = 0.4$ at the distance $y = 0.5$ mm from the wall; no flow in the wind-tunnel test section.

It should be noted that a similar asymmetry between the phases of blowing and suction was observed in a number of experiments on a flat plate (see, for example, [5]). In fact, this means that the effect of blowing on the mean flow is more significant than the effect of suction. The effect of blowing, however, dominates in the mean flow, even though blowing and suction are equally applied to the turbulent boundary layer [4]. In our case, therefore, the blowing effect, compared with suction, could be expected to be even greater.

The amplitude of the forced signal

$$A_0 = (v_f)_{\max}/U_\infty$$

was varied and amounted to $A_0 = 0.2$, 0.3, and 0.4. Some measurements were also performed for $A_0 = 0.5$. The level of circumferential nonuniformity of the forced signal amplitude was checked only for two values of the angle φ (0 and 180 deg). Within the measurement error, the values of A_0 for $\varphi = 0$ and 180 deg are almost identical.

The frequency of the forced signal in the wall units

$$f^+ = f\nu/v_*^2$$

was set to be $f^+ = 0.0051$, 0.0077, 0.0099, and 0.0126, where v_* was taken to be constant for all injection rates and equal to the value without injection. The values f^+ were selected in the following way. As previously mentioned, the dynamic loudspeaker was linked to a common settling chamber by a hose that is 28 mm in diameter. When the loudspeaker generates time-periodic forcing, this hose acts as a typical waveguide. In view of this fact, detailed measurements of acoustic oscillations at the hose output were performed at different amplitudes and frequencies of the sinusoidal signal with the use of a miniature microphone and with no flow in the test section. In other words, we varied the acoustic frequency to find the tube resonance frequency, the experimental frequency being chosen to avoid this region. The results obtained made it possible to find frequencies with a minimum level of acoustic oscillations at the hose output at these amplitudes.

The main parameters of the regular boundary layer in the cross section 13 mm upstream from the annular slot are given in Table 1.

(Here, δ_0 is the boundary-layer thickness, which is taken to be at the location at which $U/U_\infty = 0.99$, $H = \delta^*/\theta$ is the shape factor of the boundary layer, where δ^* and θ are the displacement thickness and momentum thickness

Table 1 Boundary-layer parameters in an undisturbed case

$\Delta x/\delta_0^*$	δ_0^*, mm	θ_0, mm	δ_0, mm	H	v_*, m/s	Re_θ
–4.371	2.974	2.115	12.9	1.406	0.465	1348

$$\delta^* = \int_0^\delta \left(1 - \frac{U}{U_e}\right)\left(1 + \frac{y}{R}\right)\mathrm{d}y$$
$$\theta = \int_0^\delta \frac{U}{U_e}\left(1 - \frac{U}{U_e}\right)\left(1 + \frac{y}{R}\right)\mathrm{d}y \quad (1)$$

and $\upsilon_* = \sqrt{\tau_w/\rho} = U_e\sqrt{C_f/2}$ is the friction velocity, where τ_w is the wall shear stress, ρ is the air density, and U_e is the velocity at the edge of the boundary layer.) Concerning the value of the shape factor H, the following should be noted. It is well known that lateral curvature decreases the boundary-layer thickness and increases the skin friction and shape factor (see, for example, [11]). As can be seen in our case, the shape factor is larger than that in the regular boundary layer on a flat plate and thereby displays the expected feature.

Probe traversing in the boundary layer is carried out using a remotely controlled traverse gear having three degrees of freedom; this mechanism is mounted on the sidewall of the wind-tunnel test section.

The dynamic pressure q_∞ in the freestream flow is determined from the difference between the total P_0 and static P_∞ pressure registered by a pitot-Prandtl tube mounted in the undisturbed flow. The dynamic pressure is also determined from the difference $(P_{0s} - P_{\mathrm{ts}})$ between the stagnation pressure in the settling chamber of the wind tunnel and the static pressure near the exit of the contraction.

The instantaneous velocity U at the examined point of the shear flow was measured using a DANTEC 55M single-component hot-wire constant-temperature anemometer. The setup of the anemometer apparatus includes a 55M10 hot-wire bridge with a 55D10 linearizer connected to its output. The linearized signal was fed to an E-440 L-CARD multichannel high-frequency 14-bit external A/D converter board. The digitized signal was then conveyed through a USB port to a personal computer memory. The phase reference was acquired using the same A/D converter board from the output of the signal generator. At each measurement position in the boundary layer, a total of 400,000 such data pairs were acquired and logged to a computer disk file. The total duration of each record was 5 s. This duration in terms of δ/U_∞ was 3900, to guarantee the statistical convergence of the phase averages. The value defined is comparable with the duration used in similar situations by other researchers (see, for example, [4]). The constant component of the linearized signal, corresponding to the mean flow velocity, was measured in parallel using a 55D31 digital dc voltmeter. The fluctuating signal was visually observed using a C1-73 oscilloscope. As a primary measurement transducer, a miniature hot-wire probe with a single sensor made of tungsten wire with diameter of 5 mm and active length of 1.2 mm was used. The initial position of the wire relative to the wall was determined by using a cathetometer to measure the distance between the wire and its reflection on the test surface. The estimated accuracy of this procedure is ± 2 μm.

It is known [12] that if a weakly organized (periodic) motion is superimposed on the basic turbulent motion, all fluctuating quantities [e.g., instantaneous velocity $U(x,t)$] can be presented as a sum of three components:

$$U(x,t) = \bar{U}(x) + \hat{u}(x,t) + u'(x,t) = \langle U(x,t)\rangle + u'(x,t) \quad (2)$$

where $\bar{U}(x)$ is the time-mean component, $\hat{u}(x,t)$ is the phase-averaged or coherent component, and $u'(x,t)$ is the random or incoherent fluctuation. The phase-averaged signal is defined as

$$\hat{u}(t) = \lim \frac{1}{N}\sum_{n=0}^{N} U(t + nT) \quad (3)$$

where T is the period of the forcing. At each measured position, $N = 335$–860 segments of data (depending on the forcing frequency) were averaged. Thus, because phase-averaging is used, we can identify in the overall signal both the randomly fluctuating component and the deterministic periodic motion. Hence, the root-mean-square value of the streamwise component of the velocity fluctuations and root-mean-square value of periodic velocity component were determined, respectively, as

$$u'_{\mathrm{rms}} = |\overline{(\langle U\rangle - U)^2}|^{0.5} \quad (4)$$

$$\hat{u}'_{\mathrm{rms}} = |\overline{(\langle U\rangle - \bar{U})^2}|^{0.5} \quad (5)$$

The local values of skin friction C_f for $f^+ = 0$ were determined by the Preston tube technique [13]. The value of C_f was the averaged value between those measured by the Preston tubes with outside diameters of 1.602 and 1.06 mm (47 and 31 in wall units, respectively). The initial information was processed with the use of the calibration dependence proposed by Patel [14]. Concerning the case $f^+ \neq 0$, preliminary experiments showed that none of the indirect methods available can ensure absolute reliability of determining friction in a flow, especially with significant gradients of C_f in the x direction. On the other hand, it is known that the Preston method is based on the assumption of the existence of a well-defined standard logarithmic law (law of the wall) in the turbulent boundary layer. With surface transpiration, the conventional law of the wall breaks down (see Sec. II). Therefore, Preston tubes can no longer be used if $f^+ \neq 0$. In this case, the preferable method turned out to be the direct optical method with the use of an oil drop (film) developed in [15] on the basis of a single-beam laser interferometer, which was successfully used previously in various flows ([16,17] and others). Radiation of a He-Ne laser with a wavelength $\lambda = 0.67$ μm and power of 5 mW, formed into a plane-parallel beam, was directed to the surface of an oil drop applied onto the surface of the body of revolution. The drop image modulated by interference fringes of identical width carrying information on the drop profile was recorded in reflected light by a Leutron Vision LV-8500 CCD camera with a resolution of 766×580 pixels and was then fed to a PC. After some preliminary tests, preference was given to Dow Corning 200® silicon oil with a kinematic viscosity $\nu = 50$ cS (at $t = 25°$C), density of 0.96 g/cm^3, and refractive index of 1.401. The temperature on the model surface t_w was registered by an HP Agilent 34970 data acquisition/switch unit. Because t_w changed within 0.1°C in the experiment, no allowance for the kinematic viscosity of oil was needed. From one test to another, however, the change in temperature was approximately 1°C; therefore, the true value of ν was determined with allowance for t_w variation, in accordance with the calibration curve for this oil. To improve the accuracy of friction determination, 289 interferograms of the oil drop spreading on the model surface were recorded at each examined point. Data processing was performed by a special code developed in the MatLab environment, which automatically determined the step of the interference fringes and averaged it over all 289 interferograms; otherwise, this procedure could be done using an arbitrary number of interferograms. This information, combined with data on the physical properties of oil, made it possible to uniquely determine the wall shear stress at the examined point of the flowfield on the model surface.

A detailed description of the laser interferometer skin friction technique (LISFMeter), its limitations, and its primary error sources is given in [14]. The oil viscosity that requires accurate calibration of the oil and the oil temperature that must be measured with great care are the dominant error sources. In addition, the resulting accuracy is highly susceptible to oil contamination by dust and the quality of surfacing polishing. At the same time, the primary advantage of our optical scheme is that it has relatively weak susceptibility to vibrations. Certainly, this refers to the mean value of the skin-friction coefficient. It is clear that such an approach cannot be used to measure instantaneous values of skin friction. Thus, the aforementioned requirements being satisfied, the measurement error in skin friction is largely random. Taking this fact into account, repeated experiments at a fixed surface point with periodic blowing/suction were performed in the present study. Only a minor uncertainty in the fringe locations due to the test-body vibration was actually observed. However, because the distances between the

interference fringes were averaged over a large number (several hundreds) of the interferograms, this error virtually vanished. The random measurement error of the local skin-friction coefficient was found to be within 5%.

Finally, it should be noted that the random errors in measuring the primary quantities of interest (the wall-normal distance y, the streamwise coordinate x, the pressure coefficient C_p, the dynamic pressure q_∞, the mean flow velocities U_∞ and U, the skin-friction coefficient C_f, and the velocity fluctuations u') are $y \pm 0.005$ mm, $x \pm 0.2$ mm, $C_p \pm 2.0\%$, $q_\infty \pm 0.25\%$, $U_\infty \pm 0.5\%$, $C_f - 5\%$, $U \pm 0.5\%$, and $u' \pm 2\%$.

III. Results and Discussion

To improve the measurement accuracy and obtain reliable information on the effectiveness of the flow control method used, all experiments with and without periodic blowing/suction were performed in a united set of tests. Correspondingly, the first experiments were performed in the absence of forcing, and the subsequent tests (with the model in the same position) were performed with periodic blowing/suction with varied amplitude A and frequency f. To limit the range of acceptable values of A and f, preliminary experiments were performed, aimed at studying the effectiveness of this flow control method at individual points of the flowfield.

A. Characteristics of the Regular Flow

The goal of the first experiments was to analyze the state of the regular boundary layer on the body of revolution (i.e., without local blowing/suction). The distributions of static pressure on the model surface showed that a region of a weak favorable pressure gradient ($dC_p/dx \le 0.08$ m^{-1}) is formed directly in the examined region ($0.398 \le x/L \le 0.476$), where the strongest effect of blowing/suction might be expected. Further downstream ($0.476 \le x/L \le 0.895$), a region of flow stabilization is formed, where the static pressure can be considered as constant within the experimental error.

To gain better insight into the regular boundary-layer flow, we examined the profiles of mean flow velocity and its instantaneous streamwise velocity fluctuations in detail, in the frequency band of 1–50,000 Hz, and we performed the skin-friction measurements at 15 to 20 cross sections over the length of the model. First, the mean velocity profiles for two values of the angle φ (0 and 180 deg) were measured to check the influence of three-dimensional effects in the boundary layer on the presented results. Within the measurement error, the mean velocity values, at least for $\varphi = 0$ and 180 deg, are almost identical. This means that to a first approximation, the three-dimensional effects do not play a vital part. The ratio of the boundary-layer thickness on the body of revolution to the cross-sectional radius of the body varied in the range 0.26–0.39; that is, this ratio is such that the analysis of characteristics of the shear flow could not be performed using the traditional approach applied to flat boundary layers. Therefore, our analysis takes into account the effect of lateral curvature [11]. The analysis shows that the characteristics of the undisturbed shear flow on the body of revolution completely agree with the physical concepts of the properties of a turbulent boundary layer formed on a body with lateral curvature in a nominally gradientless flow.

As an example, Fig. 3 shows semilogarithmic plots of experimental profiles of flow velocity in the boundary layer in the law-of-the-wall variables $U^+ = f(\eta^+)$:

$$U^+ = U/v_*, \qquad \eta^+ = \frac{4\eta}{(1 + \sqrt{1 + \eta/\eta_0})^2} \tag{6}$$

where $\eta = yv_*/\nu$ and $\eta_0 = Rv_*/\nu$ are the nondimensional coordinates normal to the wall and R is the radius of the cylindrical part of the body of revolution. For comparison, Fig. 3 also shows the canonical velocity profile $U^+ = A \log \eta^+ + B$ (solid curve), with the values $A = 5.62$ and $B = 5.0$, as recommended in [18], and the velocity profile in the laminar sublayer, which satisfies the condition

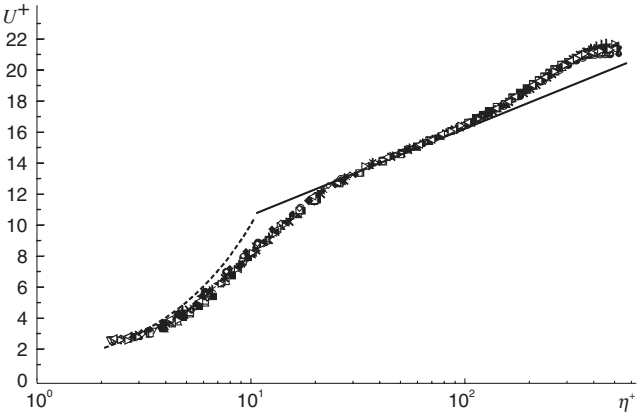

Fig. 3 Streamwise mean velocity profiles in the law-of-the-wall variables for the regular boundary layer; values x/L: ●, 0.311; ▲, 0.313; △, 0.314; ▼, 0.315; ▽, 0.316; ■, 0.317; □, 0.319; ◆, 0.321; ◇, 0.325; +, 0.329; ◁, 0.335; *, 0.342; ×, 0.354; ◀, 0.374; ▷, 0.391; and solid line, $U^+ = 5.62 \log y^+ + 5$, according to [18].

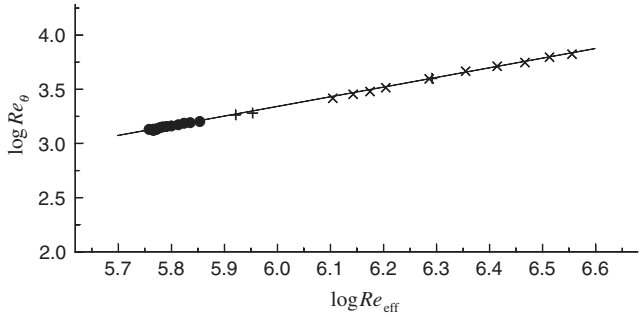

Fig. 4 Dependence $\log Re_\theta$ as a function of $\log Re_{\text{eff}}$ for the regular boundary layer; U_∞: ●, 10.1 m/s; ×, 15 m/s; and +, 25 m/s.

$U^+ = \eta^+$ (dashed curve). The experimental distribution of velocity does not contain anything unusual and agrees with the classical distribution. This allows us to conclude that to a first approximation, a developed turbulent boundary layer is formed along the model. At the same time, it can be seen that not-quite-physical behavior of experimental distribution of boundary-layer velocity is observed in the near-wall flow region. This must be attributed to wall-proximity effects. Indeed, the increased cooling of the hot wire in the vicinity of the colder wall produces higher apparent velocities. At greater distances, this results in an almost-linear velocity profile that does not pass through the origin. At small distances, wall influence predominates and the apparent velocity increases as the distance from the wall decreases.

The distributions of integral characteristics of the boundary layer (in particular, the displacement thickness δ^* and momentum thickness θ) also show the expected features of the flow. Figure 4 shows the dependence $\log Re_\theta = f(\log Re_{\text{eff}})$, characterizing the behavior of the momentum thickness θ as a function of the Reynolds number Re_{eff} based on the coordinate x_{eff}. (Here, x_{eff} is the coordinate that characterizes the virtual origin of the turbulent boundary layer. It is defined from the condition of equality at the first measuring station between the experimental value of θ and its value obtained from the Spalding procedure [19] and from a subsequent calculation in the upstream direction to the point x, where the momentum thickness is zero.) For flow velocities varied from 10.1 to 25 m/s, this dependence has a linear character, which indicates that a developed turbulent boundary layer is formed even at the lower values of the flow velocity.

Another example is the comparative data on variation of the skin-friction coefficient along the model, which are plotted in Fig. 5 as the function $C_f = f(x/L)$, where the x coordinate is counted from the nose of the body of revolution. As may be seen, the results measured by two methods agree with each other within 1% in almost the entire

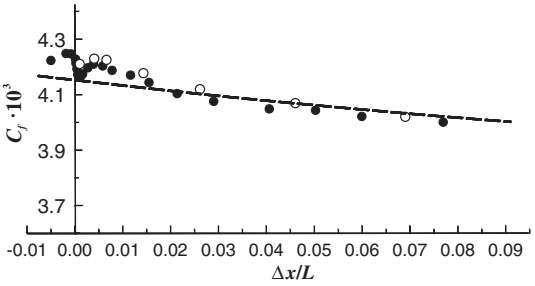

Fig. 5 Local skin-friction coefficient distribution for the regular boundary layer: ●, Preston tube method; ○, LISF; and dashed line, computation based on Cebeci's zero equation model [20].

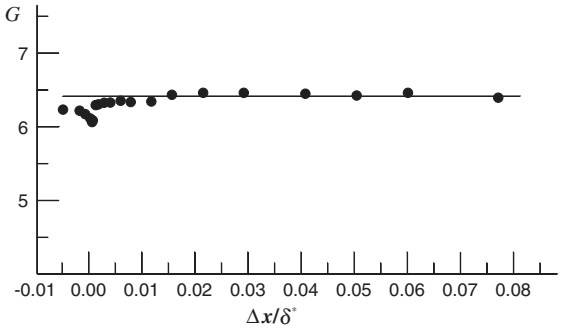

Fig. 6 Equilibrium Clauser parameter for the regular boundary layer.

examined region. We should also note fairly reasonable agreement between the experimental results and computational data (curve). These data have been obtained by a technique using the approach applied to the boundary layers. Boundary-layer equations in dimensional form for a steady incompressible axisymmetric turbulent flow can be written as

$$U\frac{\partial U}{\partial x}+\upsilon\frac{\partial U}{\partial y}=U_e\frac{\partial U_e}{\partial x}+\frac{1}{R+y}\frac{\partial}{\partial y}\left[(R+y)(\nu+\gamma_{\mathrm{tr}}\nu_t)\frac{\partial U}{\partial y}\right]$$

$$\frac{\partial}{\partial x}[(R+y)U]+\frac{\partial}{\partial y}[(R+y)\upsilon]=0 \qquad (7)$$

where $U_e(x)$ is the experimental freestream velocity distribution, γ_{tr} is the intermittency factor in the region of laminar–turbulent transition, and ν_t is the eddy viscosity. Cebeci's zero-equation model [20] was used for calculations of the eddy viscosity. The boundary-layer equations with the boundary conditions $U=\upsilon=0$ at $y=0$ and $U=U_e$ at $y\to\infty$ were solved in coupled form by a finite difference Crank–Nicolson method [21] with Newton linearization of the nonlinear term $\upsilon\partial U/\partial y$ to improve the convergence of iterations to update coefficients at each streamwise step. A Blasius boundary-layer profile was used for the initial condition. The laminar–turbulent transition was modeled by a smooth downstream modification of the intermittency factor [22]. The location of transition was chosen to exclude its influence to the flow characteristics in the region corresponding to the experimental Reynolds numbers.

It is evident from Fig. 5 that the maximum difference in C_f between the measured results and computational data does not exceed 2.7%.

It is of interest that a weak local minimum in C_f is formed in the vicinity of the slot. Apparently, the slot is, in essence, a microcavity, and both methods reveal its effect on the flow. The reason for this phenomenon can be assumed to be the specific features of the flow past a slot with a sharp trailing edge. Indeed, the Navier–Stokes computations of the flow in the vicinity of the cavity with a blunt trailing edge and a sharp trailing edge [23] show that the characteristics of the flow in the cavity proper and further downstream can be significantly different in these two cases, other conditions being identical.

The Clauser equilibrium parameter

$$G=\sqrt{2/C_f}[(H-1)/H] \qquad (8)$$

keeps an approximately constant value along the coordinate x/L (Fig. 6). There is some deviation from the equilibrium state in a direct vicinity of the slot ($\Delta x/\delta^*=0$) only, which is caused by the reason previously discussed. As a whole, $G\approx 6.4$ in a considerable length of the examined region, which is approximately 4.5% lower than the corresponding value for a flat plate under similar conditions, in which this value is 6.7 [24].

The profiles of turbulent velocity fluctuations also confirm that the characteristics of the flow around a body of revolution without blowing/suction do not contradict physical concepts on the properties of a turbulent boundary layer formed on a body with lateral

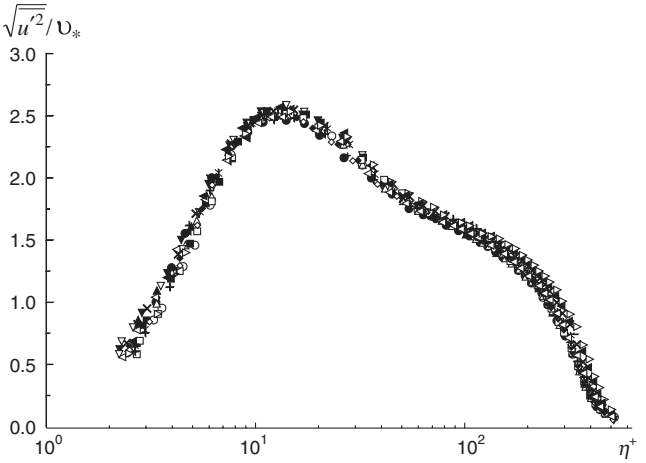

Fig. 7 Boundary-layer rms streamwise velocity-fluctuation profiles for the regular boundary layer; symbols are the same as in Fig. 3.

curvature. Indeed, as is seen from Fig. 7 [presented, like Fig. 3, in the wall variables $\sqrt{\overline{u'^2}}/\upsilon_*=f(\eta^+)$], the flow properties along the examined region are obviously self-similar. Possible underestimation of velocity fluctuations in the region of the maximum, where $(\sqrt{\overline{u'^2}}/\upsilon_*)_{\max}=2.6$, may be caused by insufficient spatial resolution of the hot-wire probe, owing to violation of the required relation between the Kolmogorov turbulence length scale and the length of the hot-wire sensor. Indeed, Ligrani and Bradshaw [25], using different hot-wire probes for measurements in the viscous sublayer at $U_\infty=7.3$ m/s, showed that the turbulent intensity is nearly independent of wire length l^+ when the latter is less than 20–25 times the viscous length scale (i.e., 20–25 wall units) and decreases significantly and abruptly for larger wire lengths. To achieve wire lengths of less than 20–25 wall units, subminiature hot-wire probes (such as those described by Ligrani and Bradshaw) with lengths as small as 150 μm are necessary for sublayer measurements in typical laboratory wind tunnels. In our case, the value l^+ accounts to about 35, and this is not enough to carry out accurate measurements of velocity fluctuations in the viscous sublayer. According to [25] the possible underestimation of velocity fluctuations in the region of the maximum can be estimated to be approximately 5.5%.

B. Effect of Local Forcing on Flow Properties

It is important to first consider pressure variation in the boundary layer. The dependence in Fig. 8 [$C_P=f(\bar{y})$, where $C_P=(P_i-P_\infty)/q_\infty$ is the pressure coefficient and $\bar{y}=y/\delta^*$ is the dimensionless wall-normal coordinate] shows the static-pressure profiles over the height of the examined region for dimensionless frequency and amplitude equal to $f^+=0.0099$ and $A_0=0.4$ and for some selected values of the streamwise coordinate $\Delta x/\delta^*$. (The data presented hereafter are normalized with the displacement thickness upstream from the slot. Symbol 0 at the δ^* is omitted for simplicity.)

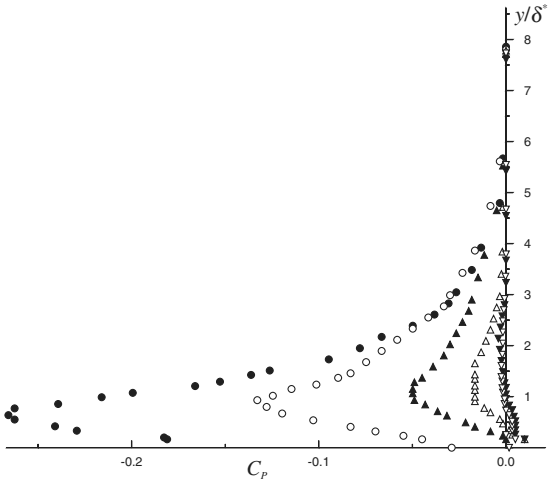

Fig. 8 Variation of static-pressure coefficient downstream of the slot for $f^+ = 0.0099$ and $A_0 = 0.4$; $\Delta x/\delta^*$: ●, 1.736; ○, 2.795; ▲, 4.234; △, 6.352; ▼, 12.703; and ▽, 23.289, where C_p values at $y/\delta^* = 0$ have been obtained from the data of orifice pressure distribution over the model surface.

The measurements were performed by a miniature static-pressure probe that is 0.7 mm in diameter, which has a hemispherical head. Some additional experiments were performed before these measurements to check if the device could be used under the conditions considered. As shown from the calibration, this probe has a region in which it is insensitive within a 1% error to flow yaw angles of ± 10 deg. In addition, some selective measurements of static pressure across the turbulent boundary layer were performed to verify the accuracy of the static-pressure probe used without blowing/suction. These measurements showed that the static pressure across the boundary layer is constant within 2%. The magnitude of the static-pressure coefficient at a normal-to-wall distance equal to the pressure-probe radius is in good agreement with that on the wall.

There is a rather significant pressure gradient, both in the streamwise and wall-normal directions (see Fig. 8), that is induced by periodic forcing. Further downstream, the character of pressure variation becomes smoother, and the pressure coefficient remains almost unchanged over the height of the examined region at a distance Δx on the order of $23\delta^*$. The results measured on the model wall ($y/\delta^* = 0$) with the help of pressure orifices are in good agreement with static pressure obtained by the probe. Concerning the wall-normal direction, the effect of periodic forcing turned out to depend mainly on the amplitude of the latter; in the case considered, the influence is bounded by the region $y \leq (5\text{–}6)\delta^*$. In addition to this, the following should be noted. As already pointed out, there are strong pressure gradients downstream of the injection slot, both in the streamwise and wall-normal directions near the wall. These gradients have opposite signs. This indicates a strong outward vertical acceleration and a streamwise acceleration in the upstream direction. This is consistent with the blowing off of the incoming boundary layer and the formation of the counterclockwise vortex shown in Sec. III.B.

One of the basic governing quantities for estimating the effectiveness of periodic blowing/suction is the local skin-friction coefficient. The results of preliminary comparative studies showed that most methods under analysis (especially empirical methods) are not very reliable in estimating the effectiveness of local forcing for flows with appreciable (over the length of the model) gradients of C_f downstream of the slot, which can be accepted in the case in which $f^+ \neq 0$. Using the optical LISF technique, we managed to ensure fairly acceptable accuracy of skin-friction measurements, owing to repeated experiments and averaging over a large number of interferograms at a fixed surface point. Thus, this method turned out to be very simple, available, and, most important, fairly accurate for determining C_f under these complicated conditions.

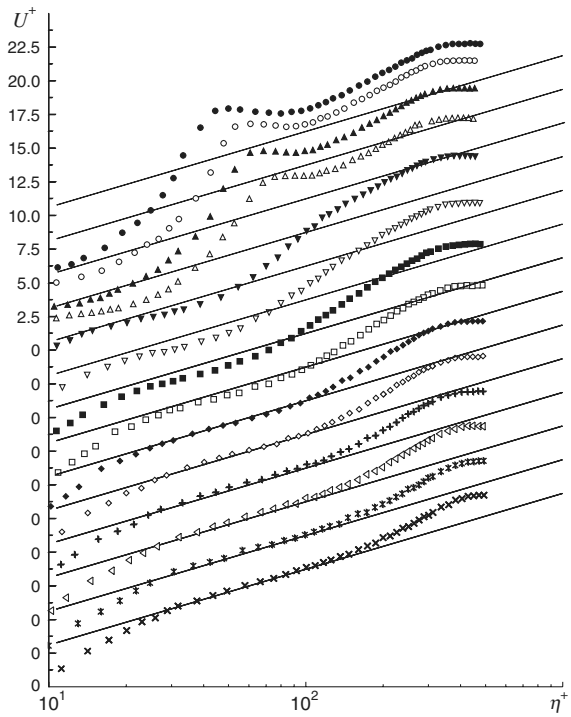

Fig. 9 Streamwise mean velocity profiles in the law-of-the wall variables downstream of the slot at $f^+ = 0.0051$ and $A_0 = 0.4$; $\Delta x/\delta^*$: ●, 0.212; ○, 0.423; ▲, 0.635; △, 0.932; ▼, 4.234; ▽, 6.436; ■, 8.469; □, 12.703; ◆, 16.938; ◇, 23.374; +, 31.758; ◁, 44.461; ∗, 65.633; and ×, 83.841.

The thus-obtained wall shear stresses (and hence friction velocity) were used to present the experimental velocity profiles in the law-of-the-wall variables $U^+ = f(\eta^+)$; an example is shown in Fig. 9 for $f^+ = 0.0051$ and $A_0 = 0.4$. As for the regular flow, the figure also contains the canonical velocity profile $U^+ = A \log \eta^+ + B$ (solid curve) with the coefficients $A = 5.62$ and $B = 5.0$ for comparison. It is worth noting that there is a retarded flow region (reduced values of velocity) near the wall at $\Delta x \leq 17\delta^*$. In the downstream direction from the slot, this region gradually moves away from the wall and almost disappears at $\Delta x \geq 23\delta^*$. At $\Delta x \cong 84\delta^*$, the disturbed velocity profiles completely coincide with the canonical profile. A similar trend was also noted in experiments [4] on a flat plate; hence, this phenomenon can serve as an indication that a flow region with reduced skin friction is formed. In addition, this fact seems to indirectly prove a more significant effect of blowing (compared with suction) on the mean flow. A similar effect was noted in [4], even for a zero net mass flux through the slot.

In addition to the results plotted in Fig. 9, we should note a substantial influence of periodic forcing on the overlap region ($1.5 \leq \log y^+ \leq 1.9$), which displays an increase in mean flow velocity and turbulent velocity fluctuations almost across the entire layer. Indeed, as it follows from Fig. 10, which shows the profiles of the root-mean-square fluctuations of the streamwise velocity component $u'_{\text{rms}}/U_e = f(y/\delta^*)$ with more detailed spacing in the Δx direction, the level of fluctuations intensely increases with distance from the slot in the downstream direction, reaching a maximum at $\Delta x/\delta^* \approx 0.6$, where the value of $(u'_{\text{rms}}/U_e)_{\max}$ is approximately 1.5 times higher than the regular value. At a distance Δx on the order of $(3\text{–}4)\delta^*$, however, the quantity $(u'_{\text{rms}}/U_e)_{\max}$ practically reaches values corresponding to a regular boundary layer, though the elevated values of u'_{rms}/U_e are still retained in the central part of the layer. This fact is undoubtedly related to flow excitation in the vicinity of the slot. At the same time, an analysis of the total instantaneous values of velocity shows that an increase in turbulent velocity fluctuations in the examined region is also caused by acoustic oscillations of the dynamic loudspeaker used. It seems necessary to pay special attention to using a source of periodic disturbances with better acoustic characteristics in further

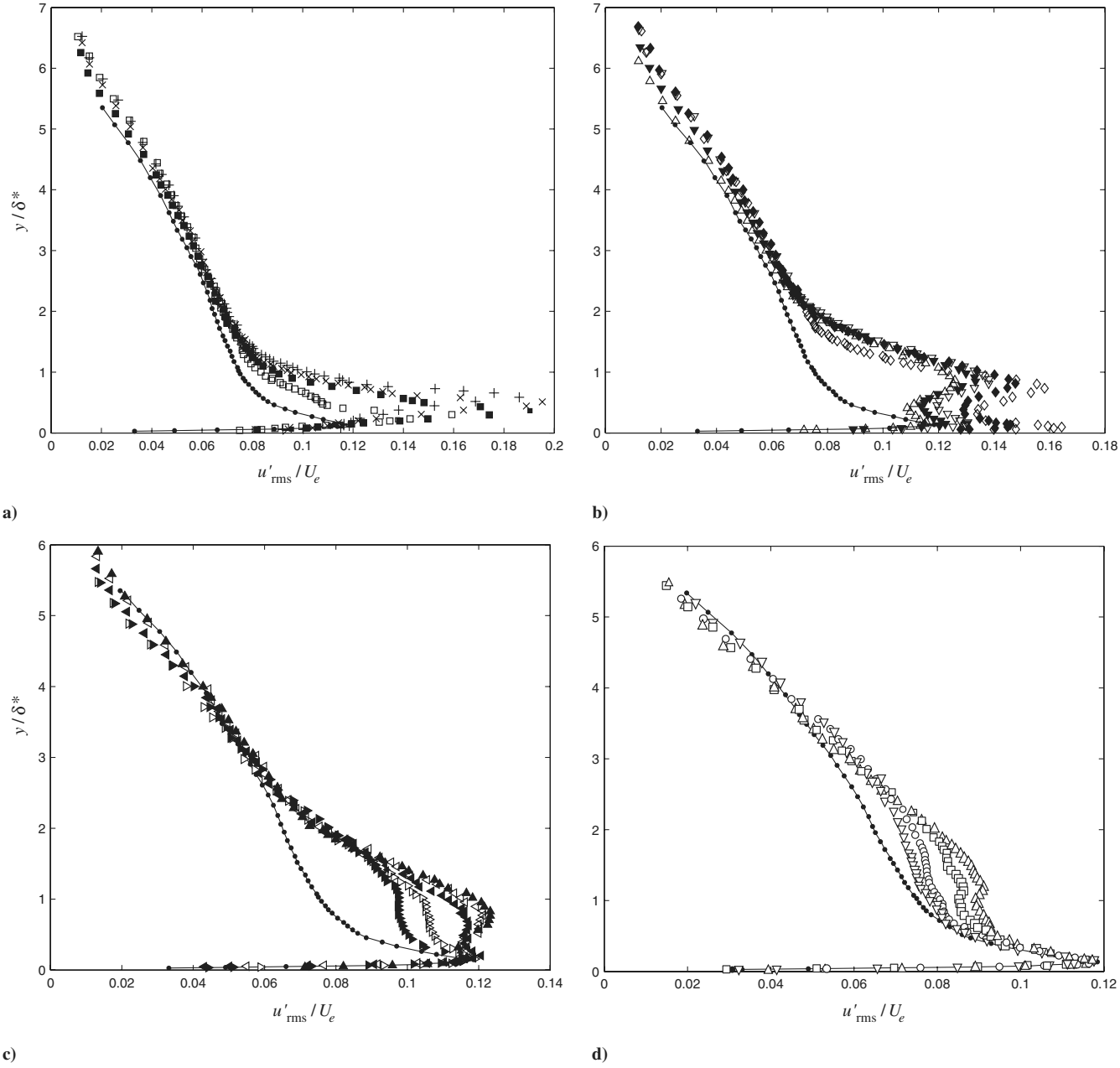

Fig. 10 Boundary-layer rms streamwise velocity-fluctuation profiles for $f^+ = 0.0051$ and $A_0 = 0.4$; $\Delta x/\delta^*$; −●−, 66.633: a) □, 0.101; ■, 0.212; ×, 0.423; +, 0.635; b) ◇, 0.932; ◆, 1.782; ▽, 2.286; ▼, 2.724; △, 3.362; c) ▲, 4.234; ◁, 5.044; ◀, 6.436; ▷, 10.087; ▶, 12.703; and d) ▽, 16.938; ○, 23.374; □, 31.758; and △, 52.118.

experiments. It is also important to note the following. The results of direct comparison of the boundary-layer velocity-fluctuation profiles in the near-wall flow region with and without blowing/suction showed that the maximum turbulent fluctuations for the case of blowing/suction is shifted substantially to the side of the larger value of wall-normal coordinate y. This means that thickening of the viscous sublayer occurs in this case.

The use of the phase-averaging procedure made it possible to obtain isocontour plots of periodic velocity component $\hat{u}(x,t)/U_e$, which are shown in Figs. 11a and 11b for $f^+ = 0.0051$ and $A_0 = 0.4$

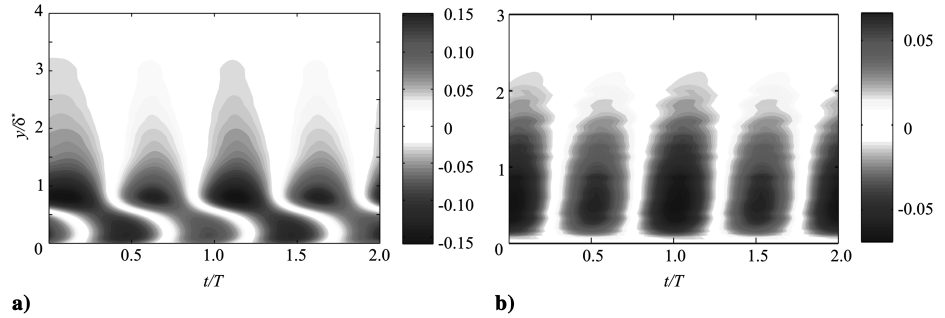

Fig. 11 Isocontour plots of periodic velocity component $\hat{u}(x,t)/U_e$ for $f^+ = 0.0051$ and $A_0 = 0.4$; $\Delta x/\delta^*$: a) 0.932 and b) 12.703.

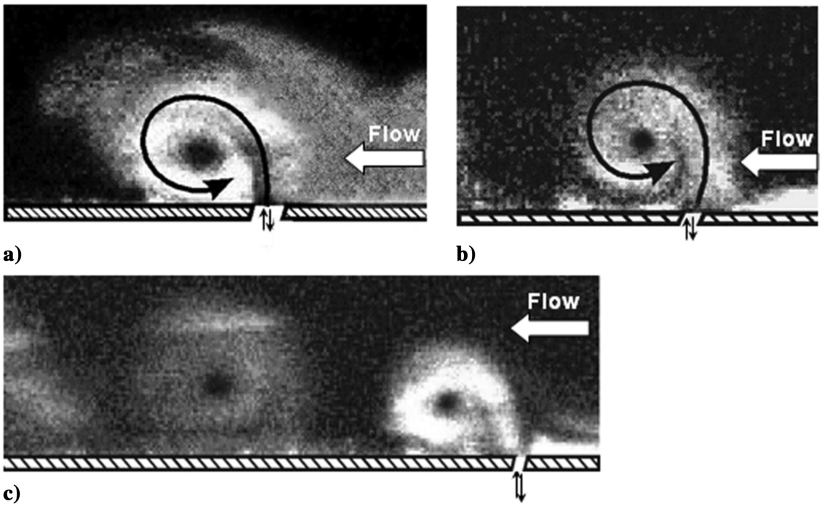

Fig. 12 Typical laser-sheet photos illustrating vortex generation behind the slot with periodic blowing/suction: a) $f^+ = 0.0099$ and $A_0 = 0.4$, b) $f^+ = 0.0099$ and $A_0 = 0.5$, and c) $f^+ = 0.0099$ and $A_0 = 0.4$. A thin laser sheet propagates along the generatrix of the body of revolution. The width of the slot is not shown to scale.

and for two values of $\Delta x/\delta^*$. In these plots, the isocontour plots are displayed on the $t/T - y/\delta^*$ plane during two periods T of the forcing. These data give grounds to believe that the flow is dominated by the presence of an unsteady coherent vortex in the near-wall flow region. An inspection with more detailed spacing in the Δx direction reveals some peculiarities in the process of vortex formation downstream from the slot. At $\Delta x/\delta^* = 0.168$, the origin of the vortex is observed in the region $0.3 \le \bar{y} \le 1.8$. As the vortex moves downstream from the slot, the growth of the vortex scale occurs (Fig. 11a) followed by its gradual reduction (Fig. 11b), so that at $\Delta x/\delta^* \ge 25$, any indication of the vortex is absent. It is worth mentioning here that an organized vortical structure was previously revealed in [4] on a flat plate in a flow region where $35 \le y^+ \le 120$. Moreover, the PIV results [6] showed that strong large-scale vortices are generated behind the slot and persist farther downstream. To obtain more reliable information in the present work, the flow was visualized by the laser-sheet technique. To provide a necessary image contrast, smoke ejection into the boundary layer through orifices located upstream of the slot was arranged. Typical photos of the flow visualization in the neighborhood of the slot are given in Figs. 12a–12c. It is seen that a toroidal vortex is actually formed in the vicinity of the slot with periodic blowing/suction. (The possible difference in the streamwise locations of the vortex centers may be attributed to the difference in phase lag between the vortex center and the slot.) Though no direct measurements characterizing the vortex-rotation direction are available, it can be assumed to be counterclockwise (marked by the arrow in the figure). Depending on the image contrast, one can easily see one (Figs. 12a and 12b), two (Fig. 12c), three, or even four toroidal vortices initiated by periodic blowing/suction. It should be noted that the forcing parameters in Fig. 12c are the same as in Fig. 12a. The experiment for Fig. 12c was undertaken to reveal more detailed vortex structures.

It is difficult to describe the quantitative aspects of these vortices from the photos. However, both the streamwise and wall-normal dimensions of the core region of the vortex can be determined. Typical wall-normal size of the core region of the vortex observed at $\Delta x = 1.2\delta^*$ was found to be about 65–70 wall units. The results obtained clearly show that with increasing distance $\Delta x/\delta^*$, this vortex gradually lifts away from the wall, its intensity decreases, and the vortex structure dissipates to a large extent. However, typical features of the existence of such a vortex with a clearly visible core can be recognized even at a distance Δx of about 30–$40\delta^*$. A closer inspection of the flow visualizations reveals that the aforementioned large-scale vortex propagates downstream with a velocity on the order of $0.8U_\infty$. In view of the foregoing, it is clear that the dominating role of the vortices mentioned in forming the near-wall flow structure is undoubted.

Isocontour plots of periodic velocity component $\hat{u}(x,t)/U_e$ on the $\Delta x/\delta^*$–y/δ^* plane for $t/T = 0$ (in respect to phase of the forcing blowing) is shown in Fig. 13 for the same amplitude and frequency parameters as in Fig. 11. These data give an additional ground to believe that the local forcing really generates an intense large-scale structure developed in the x direction in the form of a vortex. A physical explanation of this phenomenon, at least partly, may be given as follows. Indeed, at the blowing phase, the incoming shear flow seems to be temporarily blocked by a strong upwash jet flow directed from the wall through the slot. Because of that, the pressure in the flow region directly behind the slot decreases abruptly (see Fig. 8), the mainstream flow breaks up, and a recirculation region with a reverse flow is formed. The subsequent suction phase favors a further increase in stability of the counterclockwise vortex motion being formed. It is also seen that as the distance Δx increases, this large-scale inclined structure gradually lifts away from the wall and then dissipates to a large extent. Note that the inclined shape of the

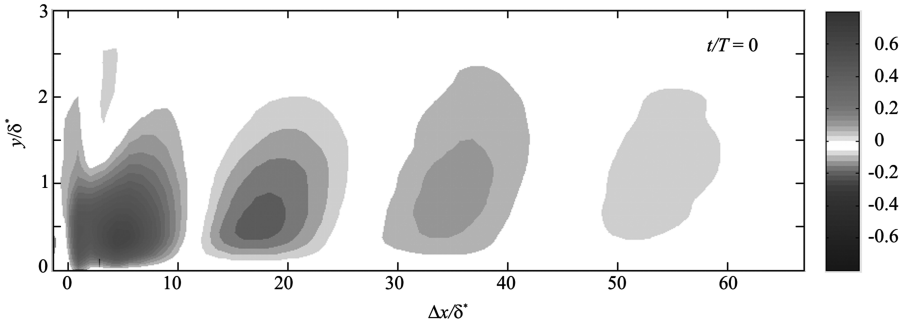

Fig. 13 Distribution of the periodic velocity component $\hat{u}(x,t)/U_e$ for $t/T = 0$ (in respect to the phase of the forcing blowing) at $f^+ = 0.0051$ and $A_0 = 0.4$.

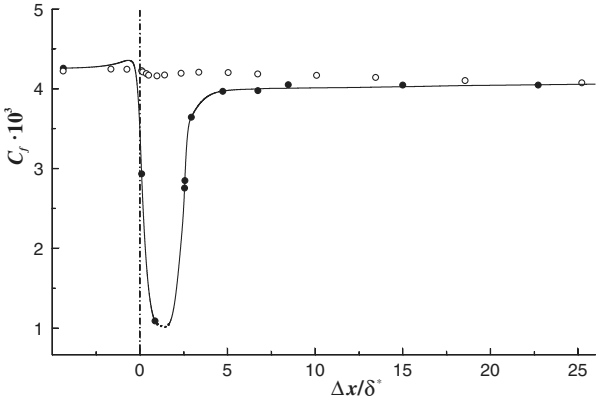

Fig. 14 Local skin-friction coefficient distribution downstream of the slot: ○, regular boundary layer and ●, forced boundary layer for $f^+ = 0.0051$ and $A_0 = 0.4$.

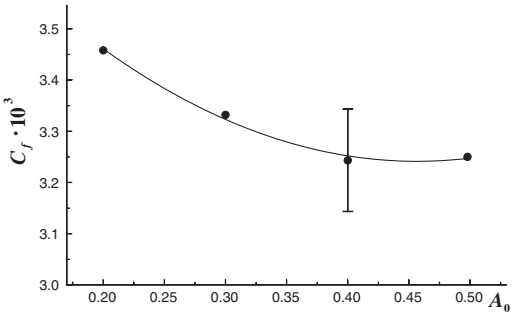

Fig. 15 Local skin-friction coefficient vs forcing amplitude for $f^+ = 0.0051$ at $\Delta x/\delta^* = 1.778$ (wall-fixed hot-wire data).

coherent structure observed here is similar to structures reported by Park et al. [4]. As a consequence, low-speed layers of the fluid are shifted upward and hence the viscous sublayer becomes thicker. This observation is obviously supported by the mean velocity profiles in the boundary layer (see Fig. 9), which clearly indicate the formation of a retarded flow region (with reduced velocity) near the wall at $\Delta x \leq 17\delta^*$. A similar trend previously observed in experiments [4] on a flat plate can testify that a flow region with reduced skin friction is formed.

It is also seen from Fig. 13 that the wall-normal size of vortices h_y increases with distance from the slot, approximately from $1.5\delta^*$ to $2\delta^*$, which corresponds to 130–170 in the wall units h_y^+. On the other hand, it was found in [4] that the wall-normal scale of vortices increases with decreasing f^+ in the range of forcing frequencies $f^+ = 0.011$–0.044 and amplitude $A_0 = 0.4$, and at the lower boundary of this frequency range, reaches a value of 88 at $\Delta x/\delta^* = 2$. (There, the scale of these vortices was not given for other values of $\Delta x/\delta^*$.) Although the range of f^+ was much smaller in our experiments, nevertheless, taking into account the trend of the h_y^+ behavior with decreasing f^+, we can note that this quantity qualitatively agrees with the data of [4]. At the same time, no significant difference in the streamwise and wall-normal sizes of the vortices being analyzed were found either.

Possibly, the vortex flow structure is even more sophisticated. A counter-rotating vortex may form in the flow region $0 \leq \bar{x} \leq 1.5$; $0 \leq \bar{y} \leq 0.5$ and is entrained by the downward motion of the primary vortex. We hope to study this issue in further experiments by using fine-resolution methods of flow visualizations.

One of the main questions arising in using periodic forcing as a boundary control method is whether it ensures local skin-friction reduction and, if so, what is the length of this region along the Δx axis. Typical results for $f^+ = 0.0051$ and $A_0 = 0.4$ are plotted in Fig. 14 as the dependence $C_f = f(\Delta x/\delta^*)$. For comparison, we also show the measurement data obtained in a regular flow ($f^+ = 0$). It is seen that C_f decreases sharply directly downstream of the slot and reaches a minimum at $\Delta x/\delta^* \approx 2$; the position of this minimum is insignificantly shifted downstream as the forcing frequency is varied. In the case presented, the maximum reduction of turbulent friction reaches approximately 70%. Further downstream, the value of C_f increases (at first, sharply, and then gradually) and approaches its value in the regular flow. In a quite wide flow region, up to $\Delta x/\delta^* = 25$, where the local friction reaches its regular state, the value of C_f remains lower than the corresponding value typical of this state.

It is of interest that there is a qualitative similarity between the distributions of some mean flow parameters behind the slot and those observed downstream of a wall-mounted fence [26]. Depending on the fence height, different reverse-flow regions can be formed behind the fence. If a strong reverse-flow region is generated, the similarity, at least qualitative, was found to exist in both static-pressure and skin-friction distributions with those behind the slot. In this case, the skin-friction coefficient decreases abruptly in the streamwise direction and reaches a negative value at the distance $x/x_R = 0.6$, with x_R being the length of the reverse-flow region. Further downstream, the value of C_f increases gradually and then remains almost constant at $x/x_R \geq 2.5$.

The function $C_f = f(A_0)$ in Fig. 15 shows similar results characterizing the effect of the forcing amplitude A_0 at $\Delta x/\delta^* = 1.778$ (i.e., outside the cross section in which the maximum friction reduction is observed). It should be noted, however, that we were not able to obtain these results by LISF technique. For this reason, they were obtained with the well-known wall-fixed hot-wire method [27]. Although the uncertainty of these results (see the vertical bar) was quite large, nevertheless, they give grounds to argue that an increase in A_0 raises the effectiveness of this flow control method to a certain extent. This is in qualitative agreement with the conclusions of [10] for the flow past a flat surface. At the same time, the use of this method of boundary-layer control at $A_0 \geq 0.40$–0.45 seems to become ineffective. In our opinion, this may be explained by the following fact. As the forcing amplitude A_0 reaches the magnitude on the order of 0.4, gradual overexcitation of the boundary layer occurs. The essence of this phenomenon is as follows. The penetrating effect of the jet flow becomes so significant that a counter-rotating vortex is generated in the flow region ahead of the angular slot. At smaller values of the forcing amplitude, this vortex is much weaker than the main vortex, and its role seems to be negligible. As the forcing amplitude increases, this secondary vortex becomes more intensive and, as a consequence, the skin friction increases. It should be mentioned, however, that these data were obtained only for one forcing frequency, and the effect of A_0 is not completely clear.

Concerning the forcing frequency, the following should be noted. We cannot definitely argue, but the results obtained here give grounds to believe that no obvious effect of f^+ on the magnitude of skin-friction reduction was found. A roughly similar trend was observed in experiments [4] on a flat plate at $\Delta x/\delta^* \geq 2$. As the authors emphasized, the largest reduction in skin friction occurred at the highest forcing frequency $f^+ = 0.044$, though the quantitative difference is small. In fact, it is clear from physical considerations that the magnitude of skin friction must depend on the vortex size and on the process of vortex interaction with the wall. In particular, as the forcing frequency decreases, the vortex center comes closer to the wall, and its interaction with the wall is expected to be more intense. In the analysis of visualization images, however, we did not observe any remarkable change in the wall-normal position of the vortex induced by changes in the forcing frequency.

Thus, the greatest skin-friction reduction is localized in a region close to the slot. The question arises of how to enlarge the region of the skin-friction reduction further downstream of the slot as much as possible. With allowance for the mechanism of skin-friction reduction, it is clear that this problem can be resolved only by finding an effective method for maintaining a stable state of the toroidal vortex as far downstream of the slot as possible. This means that the intensity of such a vortex should be maintained at the maximum possible distance downstream of the slot. It is clear that the flow turbulence with its inherent dissipative effect, which leads to breakdown or at least attenuation of coherent structures, makes this

problem difficult to resolve. The authors hope to succeed in solving this problem in the near future using the so-called cascaded flow control with feedback. The essence of this technique consists in in-phase feeding energy in the toroidal vortex at the stage when it dissipated substantially.

IV. Conclusions

An experimental study of the effectiveness of periodic blowing/suction through a transverse annular slot on the properties of the turbulent boundary layer formed on an axisymmetric body of revolution in an incompressible flow was conducted. The data obtained allow the following brief conclusions to be drawn:

1) Periodic blowing/suction is an effective means for controlling the structure of near-wall turbulence, providing a significant decrease in friction drag, compared with a similar value for the regular boundary layer. Beginning from the distance from the slot of approximately half of the boundary-layer displacement thickness δ^* and further downstream to $25\delta^*$, a stable decrease in local friction is observed; the maximum value of this decrease reaches 70%.

2) An increase in the forcing amplitude increases the effectiveness of the control method under analysis to a certain extent. Concerning the forcing frequency, the results obtained here do not give good grounds to argue that such an effect of frequency on the magnitude of friction reduction does exist. In the future, a more detailed study concerning the influence of this value on the magnitude of friction using a large range of governing conditions would benefit. The authors are currently seeking more experimental evidence to examine this aspect of the problem.

3) A decrease in local friction due to periodic blowing/suction is caused by the dominating effect of an unsteady coherent vortex formed in the boundary layer; propagating downstream, this vortex favors the upward shift of low-speed layers of the fluid, formation of a retarded flow region near the wall, and as a consequence, thickening of the viscous sublayer.

References

[1] Choi, K.-S., "Turbulent Drag-Reduction Mechanisms: Strategies for Turbulence Management," *CISM Courses and Lectures No. 415*, edited by A. Soldati, and R. Monti, Springer–Verlag, Berlin, 2001, pp. 1–52.

[2] Johnston, J. P., and Flack, K. A., "Review—Advances in Three-Dimensional Turbulent Boundary Layers with Emphasis on the Wall-Layer Regions," *Journal of Fluids Engineering*, Vol. 118, June 1996, pp. 219–232.

[3] Park, J., and Choi, H., "Effects of Uniform Blowing or Suction from a Spanwise Slot on a Turbulent Boundary Layer Flow," *Physics of Fluids*, Vol. 11, No. 10, 1999, pp. 3095–3105. doi:10.1063/1.870167

[4] Park, S-H., Lee, I., and Sung, H. J., "Effect of Local Forcing on a Turbulent Boundary Layer," *Experiments in Fluids*, Vol. 31, Oct. 2001, pp. 384–393. doi:10.1007/s003480100305

[5] Tardu, S. F., "Active Control of Near-Wall Turbulence by Local Oscillating Blowing," *Journal of Fluid Mechanics*, Vol. 439, July 2001, pp. 217–253. doi:10.1017/S0022112001004542

[6] Park, Y.-S., Park, S.-H., and Sung, H. J., "Measurement of Local Forcing on a Turbulent Boundary Layer Using PIV," *Experiments in Fluids*, Vol. 34, June 2003, pp. 697–707. doi:10.1007/s00348-003-0604-2

[7] Iuso, G., Di Cicca, G. M., Spazzini, P. G., Malvano, R., Audino, F. M., and Onorato, M., "Flat Plate Turbulent Boundary Layer Under the Action of a Periodic Forcing," *Proceedings of the 11th International Symposium on Flow Visualization*, Optimage, Edinburgh, Scotland, U.K., 2004, pp. 55–65.

[8] Sano, M., and Hirayama, N., "Turbulent Boundary Layers with Injection and Suction Through a Slit," *Bulletin of the JSME*, Vol. 28, No. 239, 1985, pp. 807–814.

[9] Kim, K., Sung, H. J., and Chung, M. K., "Assessment of Local Blowing and Suction in a Turbulent Boundary Layer," *AIAA Journal*, Vol. 40, No. 1, 2002, pp. 175–177.

[10] Kim, K., and Sung, H. J., "Effects of Periodic Blowing from Spanwise Slot on a Turbulent Boundary Layer," *AIAA Journal*, Vol. 41, No. 10, 2003, pp. 1916–1924.

[11] Smits, A. J., and Joubert, P. N., "Turbulent Boundary Layers on Bodies of Revolution," *Journal of Ship Research*, Vol. 26, No. 2, 1982, pp. 135–147.

[12] Hussain, A. K. M. F., and Reynolds, W. C., "The Mechanism of an Organized Wave in Turbulent Shear Flow," *Journal of Fluid Mechanics*, Vol. 41, Pt. 2, 1970, pp. 241–258. doi:10.1017/S0022112070000605

[13] Preston, J. H., "The Determination of Turbulent Skin Friction by Means of Pitot Tubes," *Journal of the Royal Aeronautical Society*, Vol. 58, Mar. 1954, pp. 109–121.

[14] Patel, V., "Calibration of the Preston-Tube and Limitations on its Use in Pressure Gradient," *Journal of Fluid Mechanics*, Vol. 23, No. 1, 1965, pp. 185–208. doi:10.1017/S0022112065001301

[15] Kornilov, V. I., Mekler, D. K., and Pavlov, A. A., "On the Skin-Friction Measurement Technique by One-Beam Laser Interferometer," *Proceedings of the 5th International Conference on the Methods of Aerophysical Research (ICMAR)*, July 1990, pp. 144–151 (in Russian).

[16] Kornilov, V. I., Pavlov, A. A., and Shpak, S. I., "On the Techniques of Skin Friction Measurement Using Optical Method," *Proceedings of the International Conference on the Methods of Aerophysical Research (ICMAR)*, Pt. 1, Sept. 1992, pp. 71–74.

[17] Kornilov, V. I., Litvinenko, Yu. A., and Pavlov, A. A., "Skin-Friction Measurements in an Incompressible Pressure-Gradient Turbulent Boundary Layer: Review of Techniques and Results," *Proceedings of the International Conference on the Methods of Aerophysical Research*, Pt. 1, Nonparel, Novosibirsk, Russia2002, pp. 114–119.

[18] Coles, D. E., and Hirst, E. A., "Memorandum on Data Selection," *Computation of Turbulent Boundary Layers—1968*, Vol. 2, edited by D. E. Coles and E. A. Hirst, Stanford Univ., Stanford, CA, 1969, pp. 47–54.

[19] Spalding, D. B., "A New Analytical Expression for the Drag of a Flat Plate Valid for Both the Turbulent and Laminar Regimes," *International Journal of Heat and Mass Transfer*, Vol. 5, Dec. 1962, pp. 1133–1138. doi:10.1016/0017-9310(62)90189-8

[20] Cebeci, T., *An Engineering Approach to the Calculation of Aerodynamic Flows*, Springer–Verlag, Berlin, 1999, p. 470.

[21] Anderson, D. A., Tannehill, J. C., and Pletcher, R. H., *Computational Fluid Mechanics and Heat Transfer*, McGraw–Hill, New York, 1984, p. 600.

[22] Schlichting, H., and Gersten, K., *Boundary Layer Theory*, Springer–Verlag, Berlin, 2000, p. 800.

[23] Om, D., "Navier–Stokes Simulation for Flow Past an Open Cavity," *Journal of Aircraft*, Vol. 25, No. 9, 1988, pp. 842–848.

[24] Kornilov, V. I., and Mekler, D. K., "Investigation into Boundary-Layer Memory to 2D Disturbances," *Inst. of Theoretical and Applied Mechanics*, USSR Academy of Sciences, Preprint 32-87, Siberian Branch, Novosibirsk, Russia, 1987, pp. 1–45 (in Russian).

[25] Ligrani, P. M., and Bradshaw, P., "Spatial Resolution and Measurement of Turbulence in the Viscous Sublayer Using Subminiature Hot-Wire Probes," *Experiments in Fluids*, Vol. 5, No. 6, 1987, pp. 407–417. doi:10.1007/BF00264405

[26] Fernholz, H. H., "Near-Wall Phenomena in Turbulent Separated Flows," *Acta Mechanica*, No. 4, 1994, pp. 57–67.

[27] Nitsche, W., Haberland, C., and Thunker, R., "Comparative Investigations of Friction Drag Measuring Techniques in Experimental Aerodynamics," *Proceedings of the 14th Congress of the International Council of the Aeronautical Sciences*, International Council of the Aeronautical Sciences, Stockholm, Sweden, 1984, pp. 391–403; also International Council of the Aeronautical Sciences Paper 84-2.4.1.

N. Chokani
Associate Editor